Confinement Degradation and Enhanced Microturbulence as Long-Time Precursors to High-Density-Limit Tokamak Disruptions

D. L. Brower,[1] C. X. Yu,[1] R. V. Bravenec,[2] H. Lin,[2] N. C. Luhmann, Jr.,[1] W. A. Peebles,[1] Ch. P. Ritz,[2] B. A. Smith,[2] A. J. Wootton,[2] Z. M. Zhang,[2] and S. J. Zhao[1]
[1]*Department of Electrical Engineering and Institute of Plasma and Fusion Research, University of California, Los Angeles, Los Angeles, California 90024*
[2]*Fusion Research Center, The University of Texas at Austin, Austin, Texas 78712*
(Received 11 February 1991)

Long-time precursors of order 5 times the global energy confinement time are observed for disrupting plasmas at the high-density limit on the Texas Experimental Tokamak. These precursors, occurring well in advance of any change in the plasma MHD activity, are reflected in the electron particle and heat transport along with the density fluctuation level. Enhanced microturbulence is proposed as the physical mechanism for the confinement degradation and subsequent disruption.

PACS numbers: 52.55.Pi, 52.25.Fi, 52.35.Ra, 52.55.Fa

The operating regime of any tokamak is limited by disruptive instabilities which can act to promptly terminate the discharge. For future fusion reactors, an understanding of disruptions will be important as an ability to identify and avoid them affects both machine design and operation. These disruptive instabilities generally occur at low q_a ($=2$), where q_a is the edge safety factor, or at the high-density limit of a device. Enhanced plasma radiation with increasing density due to impurities can lead to a density-limit disruption if the total radiated power P_{rad} approaches the total plasma input power P_{in}. The physical mechanism is well understood as the plasma heating is unable to sustain the level of radiating power and a disruption occurs due to a radiative collapse [1,2]. This type of operating limit, also referred to as the Murakami limit, is characterized by the ratio $\bar{n}_e R/B_T$ which increases with additional heating or lower plasma impurity content [2,3]. The parameters $\bar{n}_e$, R, and B_T correspond to the central line-averaged electron density, device major radius, and toroidal magnetic field, respectively.

However, there exist notable cases (e.g., DITE [4], ALCATOR-C [2], D-III [2], and PBX [2]) where a density limit was reached with no evidence of a radiative collapse, suggesting another disruption triggering mechanism. This limit, which is proportional to the plasma current, is referred to as the Hugill limit [2,4]. Here, the physical mechanism has not been identified although Greenwald *et al.* [2] have speculated that such a density limit is initiated by a degradation in particle confinement.

In this Letter, long-time ($\sim 5\tau_E$, where τ_E is the global energy confinement time) precursors to Hugill-limit disruptions have been identified on the Texas Experimental Tokamak (TEXT). These precursors are manifested by increases in both the electron particle and thermal transport along with broadband small-scale density fluctuations. They occur well in advance of any measurable changes in Mirnov activity which typically begin less than one energy confinement time before the discharge termination. For such disruptions, no precursor is observed in the radiated power or its profile. Modifications to the density-fluctuation characteristics provide a mechanism for the measured deterioration in the particle and energy confinement which in turn may lead to a disruption according to the scenario suggested by Greenwald *et al.* [2]. The long-time precursors, in addition to providing direct physical evidence of the processes leading to a Hugill-limit disruption, offer a means to identify and perhaps avoid such disruptions in the next generation prototype fusion reactor devices such as BPX and ITER.

The high-density operational limit for the TEXT tokamak ($R=1$ m, minor radius $a=0.26$ m) is shown in Fig. 1, where the maximum chord-averaged electron density $\bar{n}_{e,\max}$ is plotted against the plasma current I_p (i.e., Hugill plot) for hydrogen-gas-fueled Ohmic discharges with $B_T=2.8$ T. The two notable exceptions will be discussed later. This study will focus on plasmas at the high-density limit, comparing in detail disrupting and nondisrupting discharges with $\bar{n}_e \simeq 8\times10^{13}$ cm^{-3}, $I_p=330$ kA, $B_T=2.8$ T, and $q_a \simeq 3$.

Plasma particle and heat transport are evaluated by monitoring the spatial and temporal evolution of the sawtooth density and temperature perturbations. Density perturbations are measured with a high-resolution ($\Delta x=3$ cm) multichannel far-infrared (FIR) interferom-

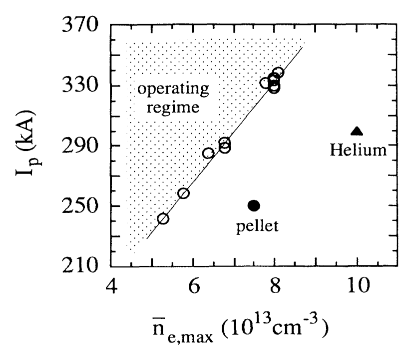

FIG. 1. Hugill plot; open circles refer to hydrogen-gas-fueled plasmas while the solid circle and triangle correspond to hydrogen-pellet-fueled and helium-gas-fueled discharges, respectively.

eter [5,6], while the temperature perturbations are estimated through use of an array of soft-x-ray detectors ($\Delta x \simeq 1.5$ cm) [7]. The transport equations are assumed simply diffusive [8] and both the "effective" electron thermal diffusivity χ_e $(=\Delta r^2/8t_p)$ and the "effective" electron particle diffusivity D_e $(=\Delta r^2/12t_p)$ are determined using the standard time-to-peak analysis in the region $0.5 \leq r/a \leq 0.8$ [6,8]. These transport coefficients ignore effects such as density-temperature coupling [7] or particle convection in the case of thermal transport. For the purposes of this paper, where only *changes* in the heat or particle transport are sought, the time-to-peak technique provides sufficient information. Multichannel heterodyne collective scattering of FIR laser radiation is utilized to measure changes in the spectra of broadband density fluctuations [9]. Since the electron particle diffusion coefficient and the density-fluctuation spectra are measured with the same FIR system (in different configurations), they cannot be determined simultaneously. However, only reproducible discharges are employed and all results have been duplicated.

The time dependences of χ_e and D_e for disrupting and nondisrupting discharges are shown in Fig. 2. One readily observes a dramatic difference in the temporal variation of the transport coefficients for the two types of discharges. For nondisrupting plasmas, χ_e and D_e are essentially constant in time during the plateau phase of the discharges. In contrast, disrupting plasmas show significant increases in χ_e and D_e well in advance of the disruption. In fact, the observed precursors occur roughly 100 ms before the discharge termination, which corresponds to roughly five energy confinement times ($\sim 5\tau_E$) on TEXT. Transport parameters D_e and χ_e change simultaneously and can increase by more than 50%. The amplitude of the sawtooth perturbations, which is used to measure the transport parameters, remains roughly constant during this time. In addition, enhanced MHD activity, as measured by external Mirnov coils, does not occur until approximately 6 ms (less than τ_E) before the termination of the discharge. Internal observations of soft x rays and the electron density indicate sawtooth activity up to the time Mirnov oscillations begin to grow. For both these discharges, the radiated power $P_{\rm rad}(r)$ is approximately half the input power and is constant in time. Once MHD instability develops, control of the plasma is lost, $P_{\rm rad}(r)$ increases, and the discharge terminates. This scenario is the same regardless of how the plasma actually becomes MHD unstable. Consequently, since there is no evidence for a precursor in the radiated power, either globally or locally, the disruption appears to be due to a Hugill limit.

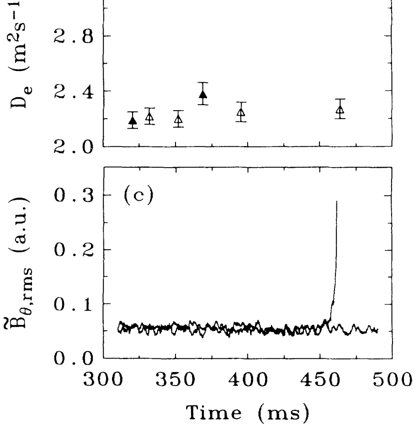

FIG. 2. Temporal development of (a) χ_e, (b) D_e, and (c) $\tilde{B}$ for disrupting (solid symbols) and nondisrupting (open symbols) plasmas. Disruption occurs at $t = 463$ ms.

If the measured transport changes are in any way driven by microturbulence, one might expect to see correlations among D_e, χ_e, and the microturbulent density-fluctuation level $\tilde{n}$. The time dependences of $\tilde{n}$ at poloidal wave number $k_\theta = 12$ cm^{-1} [i.e., $0.3 \leq k_\theta \rho_s \leq 0.9$, where ρ_s is the ion Larmor radius times $(T_e/T_i)^{0.5}$] and χ_e are shown in Fig. 3. These fluctuations are measured either above or below the midplane at the tokamak major radius. At the same time increases in D_e and χ_e are seen for the disrupting plasmas, one also observes microturbulence enhancement. Similarly, for nondisrupting discharges, the fluctuation amplitude, like the transport parameters, remains constant with time. In addition, changes of $\tilde{n}$ in the edge and scrape-off layer, as observed by Langmuir probes, occur on the same time scale as the Mirnov oscillations. Hence, $\tilde{n}$ changes observed by FIR scattering must originate in the plasma interior. Previous results from TEXTOR have also shown significant increases in the density-fluctuation level as a long-time precursor to disruptions [10].

The nature of the microturbulence modifications can be further discerned by examining the frequency spectra at various points in time prior to the disruption. The density-fluctuation frequency spectrum at $k_\theta = 12$ cm^{-1} is shown in Fig. 4(a), at a time 110 ms before a disruption. Similar observations are made for nondisrupting plasmas. Here, as for all k_θ measured (i.e., 4.5, 7, 9, and 12 cm^{-1}), the fluctuation spectra in the laboratory frame of reference are characterized by two distinct peaks which are of comparable amplitude. Previous measurements have shown that both features are seen at the plasma edge and interior, although their spatial distributions are not necessarily the same [11,12]. In the frame of the plasma, rotating due to a negative radial electric field E_r,

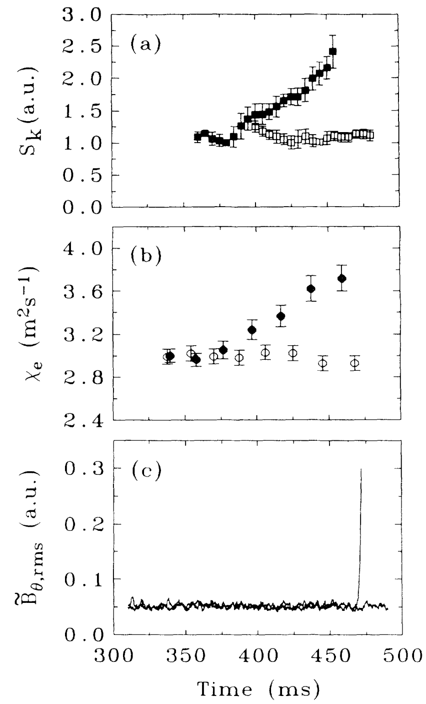

FIG. 3. Temporal development of (a) $S_k \propto \tilde{n}_k^2$ for $k_\theta = 12$ cm^{-1}, (b) χ_e, and (c) $\tilde{B}$ for disrupting (solid symbols) and nondisrupting (open symbols) plasmas. Similar observations have been made for wave numbers 4.5 $cm^{-1} \leq k_\theta \leq 12$ cm^{-1}. Disruption occurs at $t = 472$ ms.

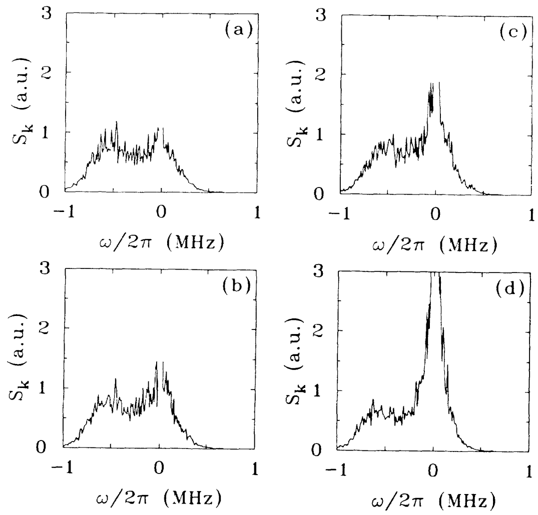

FIG. 4. Density-fluctuation level $S_k \propto \tilde{n}_k^2$ for $k_\theta = 12$ cm^{-1} at times (a) 110 ms, (b) 85 ms, (c) 52 ms, and (d) 20 ms, prior to a density-limit disruption. Disruption occurs at $t = 472$ ms.

the frequency spectra as shown would be shifted to the right with respect to the origin. Although the plasma potential profile is not known for these discharges, previous measurements on TEXT at other discharge conditions have typically found that a correction for the E_r/B_T Doppler effect is sufficiently large to shift the negative-frequency peak such that the mean frequency is comparable to the electron diamagnetic drift frequency (i.e., ~150 kHz). This fluctuation is ubiquitous and commonly associated with electron drift-wave turbulence.

The second peak occurs at $\omega \simeq 0$ but would correspond to propagation in the ion diamagnetic drift direction for a finite and negative E_r. This mode, often referred to as an ion feature, is only observed for high-density TEXT discharges, where the global energy confinement time τ_E has saturated, and has been previously put forward as evidence for ion-pressure-gradient-driven turbulence (i.e., η_i mode) [13,14]. The density-fluctuation spectra at times 85, 52, and 20 ms before a plasma collapse are shown in Figs. 4(b)–4(d), respectively. Here, it is clearly observed that while the fluctuation peak associated with the electron feature remains essentially unchanged, the ion feature has increased rather dramatically in amplitude and continues to grow right up to the disruption.

High-density discharges which disrupt due to a radiative collapse have also been studied. Such disruptions are precipitated by multifaceted asymmetric radiation from the edge (MARFE) type activity [15] where the radiated power at the smaller-major-radius edge of the torus increases significantly. These discharges have the same parameters as discussed earlier, except that the loop voltage is higher, indicating a dirtier plasma. The plasma resistivity is higher due to low-Z impurities (carbon or oxygen) and the MARFE onset occurs sharply, as evidenced by a rapid increase in the total radiated power. In this situation, P_{rad} increases prior to the plasma becoming MHD unstable and the radiated power approaches the Ohmic input power. Consequently, the associated disruptions are considered to be due to a radiation (Murakami) limit, as opposed to a Hugill limit. As expected, no long-time precursors are observed in the parameters χ_e, D_e, and $\tilde{n}$ for these density-limit disruptions.

On TEXT, consistent with the disruption scenario put forward by Greenwald *et al.* [2], degradation in plasma-particle confinement is observed for Hugill-limit disruptions. In addition, the thermal confinement also deteriorates and could be related to convective losses. A physical mechanism for the observed confinement degradation may be found in the measurements of plasma microturbulence. In particular, the specific fluctuations which propagate in the ion diamagnetic drift direction in the frame of the rotating plasma are observed to grow. If the enhanced fluctuations are related to an η_i instability [14,13], where $\eta_i = L_{ni}/L_{Ti}$ is the ratio of ion density to ion temperature scale lengths, a change in these profiles has presumably taken place. For the discharges investigated, the ion-density and temperature profiles are unknown. Earlier studies on TEXT [16] have shown that impurities accumulate in the interior for disrupting plasmas. While radiative cooling from these impurities is of minor importance [16], these small levels could potentially act to destabilize an ion-temperature-gradient–driven mode [17]. It is interesting to note that increases in $\tilde{n}$, χ_e, D_e, and impurity confinement are all associated with the core plasma.

Significant differences in the electron-density profile between disrupting and nondisrupting discharges are not evident until the plasma becomes MHD unstable. The apparent resilience of $n_e(r)$ with respect to changes in D_e suggests that the perturbative measurement of D_e may not be indicative of equilibrium transport. This result would not be surprising if the coefficients of the true transport matrix were highly nonlinear functions of the plasma profiles or a compensating pinch term were to exist [7,18]. However, confinement degradation could still be reflected in the ion channel.

The high-density limit on TEXT has been extended for two special classes of discharges as shown in Fig. 1. These are helium-gas-fueled and hydrogen-pellet-fueled plasmas. It is important to note that for both of these discharges, the ion feature in the fluctuation spectra is suppressed [13]. This correlation once again supports the notion that the measured fluctuations may be responsible for the changes in transport.

In conclusion, long-time ($\sim 5\tau_E$) precursors are observed for disrupting plasmas at the Hugill limit on TEXT, well in advance of any change in the plasma MHD activity. These precursors are reflected in the effective electron particle and heat diffusivities along with the density-fluctuation level. The proposed mechanism for this confinement degradation is enhanced microturbulence. The next generation magnetic fusion devices may be able to use these long-time precursors in order to avoid disruptions.

This research is supported by U.S. Department of Energy under Grants No. DE-AC05-78ET-53043 and No. DE-FG03-86ER-53225.

[1] J. A. Wesson *et al.*, Nucl. Fusion **29**, 641 (1989).
[2] M. Greenwald *et al.*, Nucl. Fusion **28**, 2199 (1988).
[3] M. Murakami, J. D. Callen, and L. A. Berry, Nucl. Fusion **16**, 347 (1976).
[4] P. E. Stott *et al.*, in *Proceedings of the Eighth European Conference on Controlled Fusion and Plasma Physics, Prague, 1977* (European Physical Society, Petit-Lancy, 1979), Vol. 1, p. 37.
[5] S. K. Kim, D. L. Brower, W. A. Peebles, and N. C. Luhmann, Jr., Rev. Sci. Instrum. **59**, 1550 (1988).
[6] S. K. Kim, D. L. Brower, W. A. Peebles, and N. C. Luhmann, Jr., Phys. Rev. Lett. **60**, 577 (1988).
[7] D. L. Brower *et al.*, Phys. Rev. Lett. **65**, 337 (1990).
[8] J. D. Callen and G. L. Jahns, Phys. Rev. Lett. **38**, 491 (1977).
[9] D. L. Brower, H. K. Park, W. A. Peebles, and N. C. Luhmann, Jr., *Multichannel Far-Infrared Collective Scattering System for Plasma Wave Studies,* Topics in Millimeter Wave Technology Vol. 2, edited by K. J. Button (Academic, New York, 1988), Chap. 3, p. 83.
[10] A. Boileau, H. W. H. Van Andel, M. von Hellermann, and A. Rogister, Nucl. Fusion **27**, 109 (1987).
[11] D. L. Brower *et al.*, Rev. Sci. Instrum. **61**, 3019 (1990).
[12] W. A. Peebles *et al.*, in Proceedings of the Thirteenth International Conference on Plasma Physics and Controlled Nuclear Fusion Research, Washington, DC, 1990 (International Atomic Energy Agency, Vienna, to be published).
[13] D. L. Brower *et al.*, Nucl. Fusion **29**, 1247 (1989).
[14] D. L. Brower *et al.*, Phys. Rev. Lett. **59**, 48 (1987).
[15] B. Lipschultz *et al.*, Nucl. Fusion **24**, 977 (1984).
[16] R. C. Isler, W. L. Rowan, and W. L. Hodge, Phys. Rev. Lett. **55**, 2413 (1985).
[17] G. S. Lee and P. H. Diamond, Phys. Fluids **29**, 3291 (1986).
[18] G. Rewoldt, Princeton University Plasma Physics Laboratory Report No. PPPL-2650, 1989 (unpublished).